

# Design, fabrication and characterization of a Far-field Superlens

Hyesog Lee, Zhaowei Liu, Yi Xiong, Cheng Sun, Xiang Zhang\*

*NSF Nanoscale Science and Engineering Center (NSEC), 5130 Etcheverry Hall, University of California, Berkeley, CA 94720, United States*

Received 25 May 2007; received in revised form 3 October 2007; accepted 15 October 2007 by the Guest Editors  
Available online 13 February 2008

## Abstract

The fabrication process as well as the optical characterization of a Far-field Superlens (FSL) is presented in detail. A FSL is capable of optically imaging well below the diffraction limit and works by enhancing and scattering evanescent waves to the far field which is then used to numerically reconstruct the object image [S. Durant, *J. Opt. Soc. Am. B.* 23(2006) 2383; Z. Liu, S. Durant, H. Lee, Y. Pikus, N. Fang, Y. Xiong, C. Sun, X. Zhang, *Nano Lett.* 7 (2007) 403]. We demonstrate the resolution of 70 nm gap distance of a three-line object in the far field. Also, a full optical imaging scheme, without the need for numerical processing, for a direct real-time subdiffraction-limited imaging is presented. Such remarkable imaging capability of FSL will revolutionize the optical imaging technique in the field of bio-imaging and nanolithography.

© 2008 Elsevier Ltd. All rights reserved.

PACS: 42.30.Va; 42.79.Bh; 42.79.Dj; 42.82.Bq

Keywords: A. Nanostructures; B. Nanofabrications; D. Optical properties

## 1. Introduction

Optical microscopy is the most widely used imaging method in modern scientific research. Nevertheless, conventional lens optics systems have fundamental limitations on how small a feature size can be resolved. Abbe discovered this physical barrier called “diffraction limit” a century ago [3]; even with an ideal optics system, the smallest resolvable feature is in the order of half of the wavelength used for imaging. As an object scatters incident illumination, one type of the scattered waves propagates to the far field hence it is called the ‘propagating wave’, but another type decays away near the object, which is called the ‘evanescent wave’. This evanescent wave contains high spatial frequency information that defines smaller features, but since it stays only in the near field, any far-field lenses suffer from the same diffraction limit.

Numerous efforts to overcome the diffraction limit led to breakthroughs that had or will have lasting impacts in the field of optical imaging. Near-field scanning optical microscopy (NSOM) brings a tapered optical fibre tip close

to an object and scans the region of interest pixel by pixel, delivering the evanescent information to the far field through a fiber channel [4]. Stimulated emission depletion (STED) method utilizes the nonlinear response of fluorescent dyes to create an illuminating spot smaller than the diffraction limit [5]. These methods share the serial imaging method which tends to be quite slow and requires complex illumination and detection schemes. Hyperlensing, a promising parallel imaging technique, was first experimentally demonstrated by the authors. Even though the current hyperlens showed only one-dimensional (1D) resolution improvement, there are no theoretical limitations to realizing a hyperlensing with truly two-dimensional (2D) nanoimaging in the near future [6].

Another remarkable new concept of achieving high resolution optical imaging was proposed by Pendry [7]; Evanescent fields are enhanced by a thin slab of negative refractive index material, which recovers finer details of an object and produces a perfect image. It is an unprecedented parallel imaging method with the ability to bring even the evanescent portion of the wave into focus at the image plane, collecting all spatial information of the object. Recent experimental results provided strong proofs to such controversial theory, showing an image resolution far below the diffraction limit using a flat silver slab superlens [8–10].

\* Corresponding author. Fax: +1 510 643 2311.

E-mail address: [xzhang@me.berkeley.edu](mailto:xzhang@me.berkeley.edu) (X. Zhang).

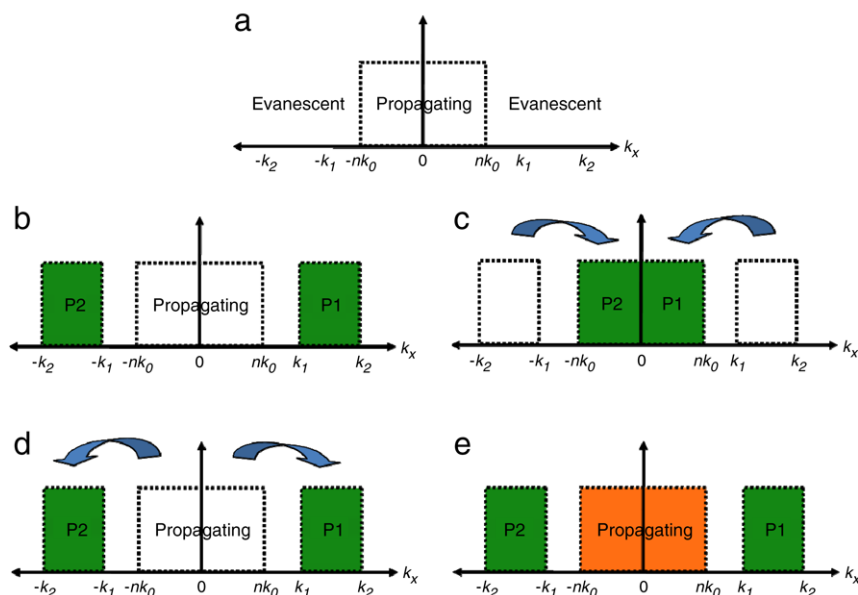


Fig. 1. Principle of FSL (Far-field SuperLenses). (a) Definition of the propagating ( $[-nk_0, nk_0]$ ) and the evanescent region ( $(-\infty \sim -nk_0]$  and  $[nk_0 \sim \infty)$ ) represented in 1D Fourier space ( $x$  axis) for simplicity. Vertical axis represents relative transfer coefficient(a.u.) (b) Evanescent bands P1 $[k_1, k_2]$  and P2 $[-k_2, -k_1]$  selected by the designed optical transfer function of a FSL are shifted into the propagating bands (c) using periodic grating structure for far-field detection. (d) Evanescent bands P1 and P2 are shifted back into their original locations. (e) Information from (d) is combined with the propagating band from an additional measurement for image reconstruction.

Later, another experiment at a longer wavelength with a silicon carbide superlens also reported similar results [11]. A major drawback of the superlensing is that it is still a near-field imaging technique [12]; The high resolution image is still confined to the proximity of the superlens surface [1].

The significance of recently proposed Far-field Superlens (FSL) theory is that it combines both of the superlensing and the far-field imaging ability, being able to image with subdiffraction-limited resolution even in the far field [1]. This direct far-field imaging became possible through a sub-wavelength grating that adds scattering functionality to the near-field superlens. This grating is specially designed such that the retrieval of the original evanescent information is possible from the far-field signal [1]. Immediately following the theoretical development, the first working FSL was experimentally demonstrated [2]. A line-pair object with 50 nm linewidth and 120 nm centre-to-centre distance was successfully imaged and resolved at half a metre away. Such achievement opened a door to a real-time far-field imaging with nanoscale resolution.

We present a detailed account of the fabrication and the characterization of a FSL. In Section 2, the design of the FSL is presented which is followed by a detailed report on its fabrication process in Section 3. In Section 4, the far-field detection scheme is presented, and the actual optical measurement and a imaging result are discussed in Section 5.

## 2. Far-field superlens design

When an object scatters incident light, the scattered waves carry spatial information of the object image. The maximum

resolution of an imaging system is determined by the largest planar wave vector collected at the image plane.

Fig. 1 schematically shows the principle of the FSL theory in a nutshell. The horizontal axis represents the inplane spatial frequency (wave vector) of the scattered waves by an object. For simplicity, only 1D coordinate is used. The vertical axis shows relative intensity level in arbitrary unit. The band bounded by  $[-nk_0, nk_0]$ , where  $n$  is the refractive index of the surrounding medium and  $k_0 = 2\pi/\lambda$  ( $\lambda$  is the wavelength in free space), is the propagating band (Fig. 1(a)) and accessible by conventional optics. However, the waves in the evanescent band (Fig. 1(a)) with larger wave vectors (i.e. carries finer spatial information of the object) tend to decay away and are accessible only in the near field [8–11].

A FSL is able to select a certain evanescent bands, for instance, P1 $[k_1, k_2]$  and P2 $[-k_2, -k_1]$  in Fig. 1(b) according to the designed optical transfer function (OTF) [1,2], and to shift them into the propagating region so that they can be detected in the far field (Fig. 1(c)). It is well known in optics that periodic structures can provide additional planar momentum to interacting electromagnetic waves. Therefore, a specially designed grating structure in a FSL provides just enough momentum to move the selected bands to the propagating region. Once the information is collected in the far field, those bands can be shifted back to their original positions through numerical processes (Fig. 1(d)), and by combining with normally attainable propagating information (Fig. 1(e)), an image with much higher resolution can be reconstructed. It should be noted that the retrieved bands are not continuous with the propagating band. However, applying a grazing angle incident light or a structured illumination [13] can close such gaps, and even without such methods, it is reported that

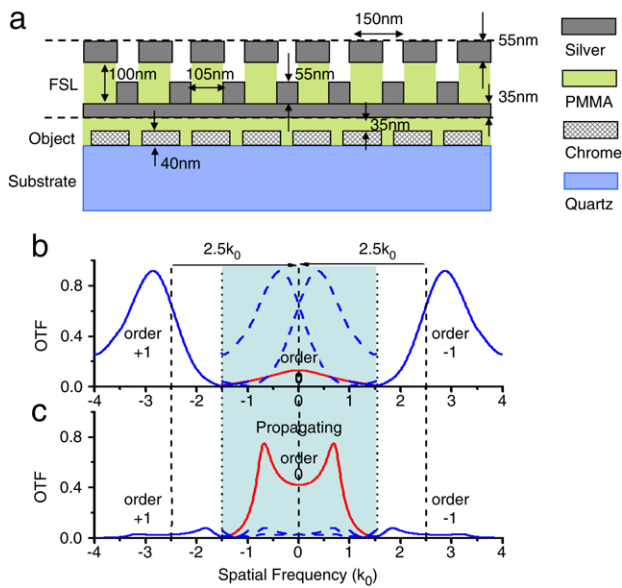


Fig. 2. (a) Designed FSL sample structure. A 40 nm thick chromium periodic object and the FSL were fabricated in the same substrate spaced by a thin polymer (PMMA) layer (35 nm). The FSL consists of silver gratings of 150 nm period on top of a 35 nm thick flat silver film. (b) The optical transfer function (OTF) of the designed structure under P-polarization of 377 nm illumination. The solid blue curve represents enhanced evanescent bands corresponding to P1 and P2 in Fig. 1(b). The dotted blue curve represents those bands after shifting by the FSL grating corresponding to P1 and P2 in Fig. 1(c). 150 nm period FSL grating enables  $2.5k_0$  shift. (c) The OTF of the designed structure under S-polarization of 377 nm illumination shows strong 0 order transmission (red curve) as expected from the propagating region in Fig. 1(e). (For interpretation of the references to colour in this figure legend, the reader is referred to the web version of this article.)

the retrieved bands produced significantly improved image resolution well below the diffraction limit [2].

Fig. 2(a) shows the configuration of our FSL sample. The sample is comprised of two main parts; an object, and a FSL, as indicated in the figure. The FSL consists of a grating structure as mentioned above and a flat silver slab. The objects are 1D metallic gratings. Since such an object represents only a very narrow band of Fourier components centred at  $k_{\text{obj}} = 2\pi/\Lambda_{\text{obj}}$ , where  $\Lambda$  is the period, various objects with different periods have been fabricated in order to characterize the transmission dependence of our FSL on the wave vectors, which is how the experimental OTF was obtained. By using the obtained OTF, a line pair [2] and a three-line object with subdiffraction-limited distances have also been resolved, which will be discussed later.

Fig. 2(b) and (c) are calculated OTFs of our designed structure shown in Fig. 2(a) under p and s polarized illumination of 377 nm respectively. Rigorous coupled wave analysis (RCWA) was used for OTF calculation and the details are discussed elsewhere [1]. Under p-polarization (Fig. 2(b)),  $-1$  and  $+1$  order diffraction bands are enhanced (solid blue) due to surface plasmon excitation at silver surface [8–10,14]. Then, the periodicity of the FSL grating provides momentum shift of  $k_{\text{FSL}} = 2.5k_0$ , which was chosen at the onset of surface plasmon enhancement band in order to minimize the overlapped area after the two bands are shifted [1,2]. Since the

scattering by a grating involves diffracting into many different orders according to  $k = k_0 + nk_{\text{FSL}}$  where  $n$  is integer grating order, one wave vector signal captured in the far field is actually a combination of the partial contributions from many different orders, which makes it impossible to retrieve the original information of an object. Therefore, one-to-one mapping is needed between the spatial frequency vectors of an object and the measured signal. An essential function of the FSL shown in Fig. 2(a) is its ability to diffract only one dominant order to the far field while suppressing all others [1,2]; one of the two dotted curves always has a dominant transmission for any spatial frequency in the propagating band (blue shaded region in Fig. 2(b)) except a small region near  $k_x = 0$  [1,2], where  $-1$  and  $+1$  order has rather significant overlap. This small region was excluded in the imaging process which did not have major affect in the image reconstruction result [2]. The zero order transfer function (red curve in Fig. 2(b)) value is always small enough that such contribution was considered negligible. This generates one-to-one information mapping between the original and the scattered signal which makes unique retrieval of spatial frequency bands of an object possible from far-field measurement. In addition, even though the diffraction-limited band (0 order transmission) is suppressed by the FSL structure under P-polarization, but this information can be obtained using S-polarized illumination as shown in Fig. 2(c). By combining the information from the p and s polarization, a complete image can be reconstructed.

### 3. Far-field superlens fabrication

A FSL needs to be placed within the near field of an object in order to capture the decaying evanescent waves. Since it is more convenient to keep a FSL at a constant distance and a laterally fixed position relative to the object during experiments, both of the FSL and the object were fabricated as one structure with a thin polymer spacer between them (Fig. 2(a)). In real imaging applications, objects can be simply placed on a FSL.

Fig. 3 summarizes the overall fabrication process, which started with patterning of the object. A 40 nm thick chromium (Cr) layer was deposited using electron beam evaporation (SLOAN) on a quartz wafer (0.5 mm thick). Grating objects were, then, inscribed into the Cr film by Focused Ion Beam (Strata FIB 201, FEI Co.) in which accelerated Gallium atoms mill grooves directly on the metal surface. The groove dimensions were 40 nm in width and 14  $\mu\text{m}$  long, and the grating period ranged from 120 to 180 nm. An entire area of an object was approximately 14  $\mu\text{m} \times 14 \mu\text{m}$ .

Before a FSL was fabricated over the object, a spacing layer was needed. The purposes of this layer were to planarize and eliminate the surface modulations of grating objects, and to keep the distance between the object and the FSL within the near-field to prevent significant decay of evanescent field. First, the surface modulations were reduced through multiple spin coatings of PMMA (495 A4, Microchem Inc.), in which 700 nm thickness was achieved in four coatings. Since spin coating is a semi-conformal deposition process [15], the peak-to-valley distance of gratings was effectively reduced. It was

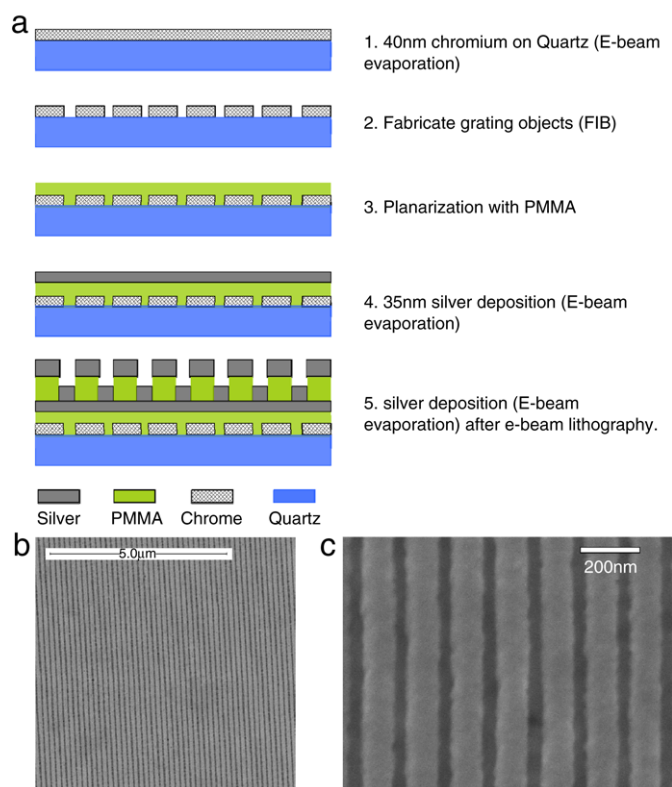


Fig. 3. (a) The FSL/object sample fabrication process. The object was fabricated by an FIB milling on a 40 nm thick Cr film. Then, a spacing layer (35 nm PMMA) was deposited to reduce surface modulation and to keep the FSL and the object in close distance (35 nm). The FSL was made by first depositing thin (35 nm) silver film as the evanescent wave enhancement layer, and second, patterning and depositing silver gratings (55 nm thick) using electron beam lithography. (b), (c) SEM pictures of the top surface after final silver deposition.

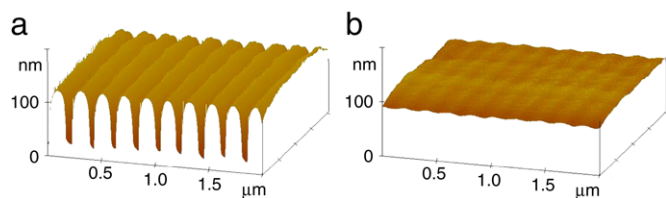


Fig. 4. Effectiveness of our planarization technique. AFM (Atomic Force Microscopy) scans of (a) a periodic metal structure before planarization having close to 100 nm peak-to-valley distance and (b) after the planarization process. The surface of 35 nm PMMA layer shows dramatically reduced 1–3 nm peak-to-valley distance and better than 0.5 nm RMS roughness.

crucial to evaporate most of the solvent in each layer with a bake (5 min at 150 °C) to ensure that the additional layer was independently coated on a hardened surface without solvent mixing. Then, Tegal plasma etcher was used to etch the PMMA layer down to 35 nm. The etching rate was measured to be 60 nm/min at 200 W power setting. Because the etching rate increased rapidly after longer etching times (>5 min) due to elevated chamber temperature, multiple short-term etching method was used for better process control. The thickness is measured between the short etching steps using Filmtek 2000 optical thickness measurement system. After the

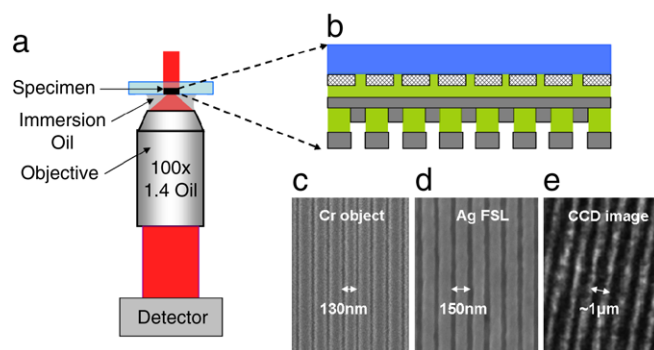


Fig. 5. (a) Far-field detection setup. The light source ( $\lambda = 377$  nm) was incident from the substrate side of the sample (b) and an optical microscope with 1.4NA oil objective was used. (c) SEM images of the Cr metal object with 130 nm period and (d) Ag FSL grating designed to have 150 nm period. (e) Recorded CCD image with measured  $\sim 1$   $\mu$ m period.

desired thickness was reached, the sample was baked above the glass transition temperature ( $T_g$ ) of PMMA (105 °C) for 30 min (190 °C hotplate). This ‘reflowing’ step reduced the surface roughness generated by plasma etching. In Fig. 4, this planarization technique was tested on a periodic metal structure with deeper grooves (100 nm) than that of the objects. It shows the effectiveness the process where the 100 nm peak-to-valley distance (Fig. 4(a)) was dramatically reduced to 1–3 nm (Fig. 4(b)). Final thickness of PMMA was only 35 nm with a remarkable roughness control of better than 0.5 nm RMS.

Then, the FSL structure was fabricated on top of the planarized PMMA layer. First, a 35 nm silver film was deposited by electron beam evaporation (SLOAN). Relatively faster deposition rate was used (>5 nm/s) in order to achieve minimum RMS roughness on the surface to reduce scattering loss. Next, the FSL grating structure was patterned using electron beam lithography with PMMA (495 A3, Microchem inc). It was spin coated on the silver surface to 100 nm thickness and the entire sample was soft-baked at 95 °C for one minute. If the baking time was too long or the baking temperature was higher than 105 °C ( $T_g$ ), the spacing layer became unstable and affected the stability of the silver film as well. After the pattern exposure, it was developed for 32 s in MIBK:IPA = 1:3 mix. Then, 55 nm thick silver was deposited using e-beam evaporation (SLOAN). This additional silver layer was designed to provide further attenuation of 0 order transmission (i.e. the propagating component). Fig. 3(b) and its magnified image, Fig. 3(c), are SEM (scanning electron microscopy) pictures taken after the final step of FSL fabrication. The final silver film on top of PMMA is shown as wider and brighter region and the darker narrow ridges are the silver gratings on top of the bottom flat silver layer. Its grating period is shown to be 150 nm as designed.

#### 4. Far-field imaging

Fig. 5(a) shows the experimental setup. A fabricated FSL/object combination sample (Fig. 5(b)) was placed under an optical microscope with a 1.4NA oil immersion objective. A laser with 377 nm wavelength (Coherent RADIUS 375–8) was

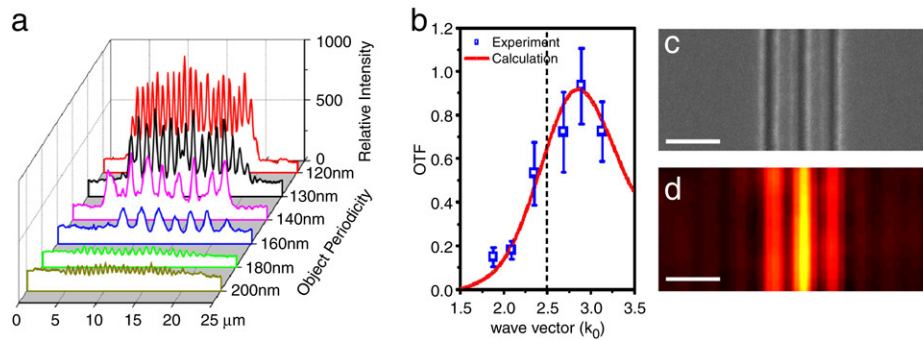


Fig. 6. (a) Relative intensity cross-section of images recorded by CCD vs. various object periods. (b) Experimental (blue squares) and calculated (red curve) OTFs plotted against lateral wave vectors show good agreement. SEM image (c) and the FSL reconstructed image (d) of a testing three-line object. The line width is 50 nm and the centre distance is 120 nm between each line. The scale bar represents 200 nm in both (c) and (d). (For interpretation of the references to colour in this figure legend, the reader is referred to the web version of this article.)

used to illuminate the sample and its transmission image was measured by a UV sensitive CCD detector (Roper Scientific).

Fig. 5(c) and (d) are SEM images of a 130 nm period object and a FSL grating. From the simple grating law,  $\frac{1}{\lambda_{\text{detected}}} = \frac{1}{\lambda_{\text{obj}}} - \frac{1}{\lambda_{\text{FSL}}}$ , the period of a captured image ( $\lambda_{\text{detected}}$ ) was calculated to be 975 nm. The measured image period of 1  $\mu\text{m}$  (Fig. 5(e)) is consistent with the calculated value. This result can be explained as a near field moiré effect where a simple wave vector mixing of two periodic structures generates another periodic image [16]. However, the uniqueness of a FSL imaging comes from its ability to selectively enhance a certain evanescent band (i.e. spatial frequency dependent optical-transfer function) necessary for the retrieval of the original wave vector information [1]. The relative intensities of the real images captured by the CCD vs. the object periodicities are plotted in Fig. 6(a). In Fig. 6(b), the spatial frequency dependent transmission behaviour of the FSL is plotted against the wave vector of each grating object based on the data shown in Fig. 6(a). The experimental OTF (blue squares) is compared with the theoretical calculation (red curve), which shows close agreement with each other even though the experimental OTF shows rather smooth but acceptably transitional cut-off in reference to the ideal sharp cut-off (vertical dotted line) at  $2.5k_0$ . This selective enhancement behaviour is an essential function of FSL generating one-to-one mapping between the measured and the original information [1].

## 5. Image reconstruction

After the experimental verification of the OTF, an object with broader spectrum was fabricated and imaged with a FSL. Fig. 6(c) shows the SEM image of a three-line object with centre-to-centre distances of 120 nm. Using the FSL, the scattered signal was captured in the far field and the original object image was numerically reconstructed (Fig. 6(d)) which showed the clearly resolved three-line object. It is possible to resolve even smaller objects since the enhancement band extends to  $4k_0$ , which represents feature sizes below 100 nm.

The image reconstruction can be done in real-time without using numerical methods as we discussed in our previous work [2], by combining information from both p (representing

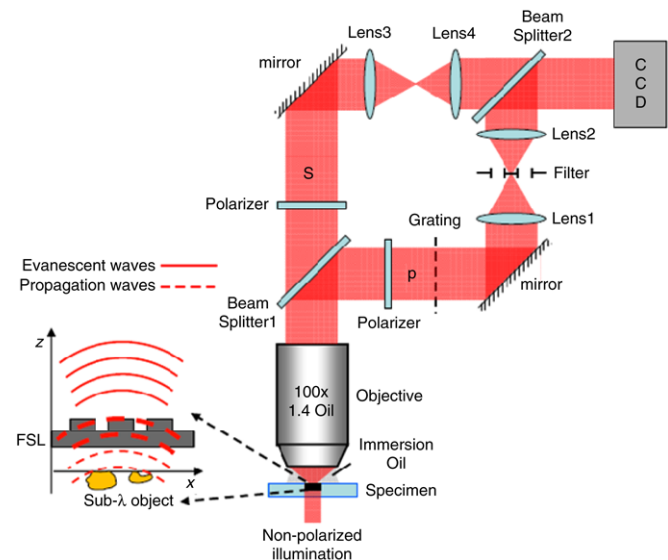


Fig. 7. Schematic setup to realize real-time image reconstruction by optics. Two polarizations which carry different information of the object can be separated by beam splitter 1 and modified individually. The final magnified subdiffraction-limited image can be obtained by recombining both polarizations.

evanescent information) and s polarization (representing propagating information) in one optical setup shown in Fig. 7. As an object scatters nonpolarized incident light, the p-polarized evanescent portion (P1 and P2 bands in Fig. 1) is enhanced and scattered by the FSL grating. Considering the microscope objective NA value of 1.4, the P1 and P2 bands (Fig. 1(b)) collected by this objective  $|k| < 1.4k_0$  originally come from the evanescent band,  $2.5k_0 < |k| < 3.9k_0$ . In addition, because the objective has 100 times magnification, the propagating wave vectors are compressed by 100 times and become  $|k| < 0.014k_0$ . Then, P1 and P2 can be shifted back to  $0.025k_0 < |k| < 0.039k_0$  by first order diffraction of a grating with the period of 100 times larger than the FSL grating. The 0 order diffraction of this grating can be filtered out at the Fourier plane, between Lens 1 and Lens 2. The initial object information  $2.5k_0 < |k| < 3.9k_0$  carried by the p-polarization are finally converted into band  $0.025k_0 < |k| < 0.039k_0$ .

Since there is no field enhancement involved for s-polarization, all of the evanescent information is negligible. Therefore, the propagating waves with  $|k| < 1.4k_0$  are converted into the band  $|k| < 0.014k_0$  just as a conventional microscope does and a filter or a screen can be placed at the Fourier plane between Lens 3 and Lens 4 to selectively control the contribution of the s polarization to the final image. The  $p$  and  $s$  information are then combined at the CCD image plane to give a subdiffraction-limited image of the object.

## 6. Conclusion

A promising nanoscale imaging method called FSL imaging was developed and experimentally demonstrated. A FSL not only enhances but also projects evanescent wave to far field, enabling a subdiffraction-limited imaging. The detailed fabrication process and the optical characterization were presented and discussed. Object with 70 nm gap distance and 120nm centre-to-centre distance was resolved in the far field. A novel FSL optics setup was proposed which enables real-time nanoscale imaging in the far field without the use of any numerical reconstruction algorithm. The FSL concept presented in this report is not limited to 1D imaging only. We have also developed a FSL capable of true 2D imaging which will be published elsewhere. The FSL opens the door to overcome the diffraction limit [2] and has potential applications in high resolution real-time bio-imaging and nanoscale lithography also with the possibility to work in various wavelengths [17].

## Acknowledgements

This research is supported by the Center for Scalable and Integrated Nanomanufacturing (SINAM), and NSF Nanoscale Science and Engineering Center (NSEC) under award no. DMI-0327077, and Army Research Office MURI program (grant no. 50432-PHMUR).

## References

- [1] S. Durant, J. Opt. Soc. Am. B. 23 (2006) 2383.
- [2] Z. Liu, S. Durant, H. Lee, Y. Pikus, N. Fang, Y. Xiong, C. Sun, X. Zhang, Nano Lett. 7 (2007) 403.
- [3] E. Abbe, Arch. Mikroskop. Anat. 9 (1873) 413.
- [4] E. Betzig, J.K. Trautman, T.D. Harris, J.S. Weiner, R.K. Kostelak, Science 251 (1991) 1468.
- [5] S.W. Hell, Nat. Biotechnol. 21 (2003) 1347.
- [6] Z. Liu, H. Lee, Y. Xiong, C. Sun, X. Zhang, Science 315 (2007) 1686.
- [7] J.B. Pendry, Phys. Rev. Lett. 85 (2000) 3966.
- [8] N. Fang, H. Lee, C. Sun, X. Zhang, Science 308 (2005) 534–537.
- [9] H. Lee, Y. Xiong, N. Fang, W. Srituravanich, S. Durant, M. Ambati, C. Sun, X. Zhang, New J. Phys. 7 (2005) 255.
- [10] D.O.S. Melville, R.J. Blaikie, Opt. Express. 13 (2005) 2127.
- [11] T. Taubner, D. Korobkin, Y. Urzhumov, G. Shvets, R. Hillenbrand, Science 313 (2006) 1595.
- [12] V. Podolskiy, E.E. Narimanov, Opt. Lett. 30 (2005) 75.
- [13] M.G.L. Gustafsson, J. Microsc. 198 (2000) 82.
- [14] Z. Liu, N. Fang, T.J. Yen, X. Zhang, Appl. Phys. Lett. 83 (2003) 5184.
- [15] L.E. Stillwagon, R.G. Larson, Phys. Fluids A 2 (1990) 1937.
- [16] Z. Liu, S. Durant, H. Lee, Y. Xiong, Y. Pikus, C. Sun, X. Zhang, Opt. Lett. 32 (2007) 629.
- [17] Y. Xiong, Z. Liu, S. Durant, H. Lee, C. Sun, X. Zhang, Opt. Express 15 (2007) 7095.